Journal of the European Ceramic Society 44 (2024) 5449–5459

Contents lists available at ScienceDirect

Journal of the European Ceramic Society

journal homepage: www.elsevier.com/locate/jeurceramsoc

Alkali activation-induced cold consolidation of waste glass: Application in organic-free direct ink writing of photocatalytic dye destructors

Mokhtar Mahmoud [a,b,c], Jozef Kraxner [a], Akansha Mehta [a], Hamada Elsayed [b], Dušan Galusek [a,d], Enrico Bernardo [b,*]

[a] FunGlass, Alexander Dubček University of Trenčín, 91150 Trenčín, Slovakia
[b] Department of Industrial Engineering, University of Padova, 35131 Padova, Italy
[c] Department of Glass Research, National Research Centre, Egypt
[d] Joint Glass Centre of the IIC SAS, TnUAD and FChFT STU, 91150 Trenčín, Slovakia

ARTICLE INFO

Keywords:
Porous glass microspheres
Alkali activation
3D scaffolds
Additive manufacturing
Photocatalytic degradation

ABSTRACT

Additive manufacturing, with its ability to assemble a variety of materials in complex and customized architectures, is developing rapidly. The integration of technologies and materials into a sustainable production, however, is still challenging. The present investigation offers new functional glass-based products, from nearly room temperature processing, based on direct ink writing (DIW) of pastes from 'light' alkali activation (2.5 M NaOH) of pharmaceutical glass waste, added with 20 wt% of TiO_2 nanoparticles. The inks were refined by the inclusion of porous glass microspheres (PGMs, 20–30 wt%), previously fabricated from fiber glass waste. Printed scaffolds, stabilized by simple drying (i.e. 'unfired'), were successfully applied in the photodegradation of methylene blue. The degradation efficiency reached 100% within 75 min, and the 3D-printed composites could be easily separated from the solution for subsequent reuse. The degradation efficiency declined only by 7.5%, after 5 cycles.

1. Introduction

Glass is a relatively challenging raw material for additive manufacturing, which can be realized by operating with melts (direct extrusion), powders (ink-jet printing, selective laser sintering), and slurries (nano- and micro-sized particles suspended in photocurable liquid) [1–3]. Difficulties with additive manufacturing of glass are related to several factors, including brittleness of glass and its sensitivity (for many formulations) to thermal shock, upon thermal processing. Significant complications may arise from the delicate trade-off between densification and viscous flow during sintering of printed glass structures. Too high processing temperatures can cause merging of adjacent particles into a nearly pore-free mass, but the overall shape may be lost due to accelerated viscous flow; in addition, the sensitivity to crystallization upon reheating may put further constraints to the processing temperature range [4].

3D printing technologies are interesting also in the perspective of reusing discarded glass fractions ('waste glass'). Cullet, i.e. material from the dismantled of glass articles, may validly replace mineral raw materials, in a new production cycle, only if adequately purified; for some glass articles, such as LCD displays, the need for absolute control on optical quality actually discourage recycling [4]. New glass-based products, quite different from the original ones, appear as the only solution for valorization of waste glass; sintering, instead of remelting (as typically occurring with glass foams) is advantageous to reduce energy demands [5]. Glass from dismantled LCD displays is actually favoured, in the sintering of 3D printed powder bodies, by characteristic features, such as stability against crystallization and 'length', i.e. a relatively large gap between glass transition and softening temperatures. This enables the densification of 3D printed highly porous scaffolds, after the removal of organic binders, without a pronounced viscous collapse [4].

The use of additives for printing and heat treatments for debinding and sintering raises important sustainability concerns. Plant-based, renewable binders and reduced sintering temperatures are considered as possible improvements. However, a dramatic enhancement of sustainability is envisaged only by complete removal of organic binders and by avoiding high temperature processing. In this perspective, the activation of glass powders with low molarity alkaline aqueous solution

* Corresponding author.
E-mail address: enrico.bernardo@unipd.it (E. Bernardo).

https://doi.org/10.1016/j.jeurceramsoc.2023.12.023
Received 3 August 2023; Received in revised form 11 November 2023; Accepted 6 December 2023
Available online 8 December 2023

Table 1
Chemical composition of the investigated waste glasses in wt%.

Oxides	SiO_2	CaO	Al_2O_3	B_2O_3	Na_2O	K_2O	MgO	TiO_2	Fe_2O_3
Pharmaceutical glass waste	72.70 ± 0.8	1.10 ± 0.03	6.70 ± 0.1	10.07 ± 0.05	7.50 ± 0.2	1.57 ± 0.03	0.31 ± 0.02	0.02 ± 0.01	0.02 ± 0.01
Fiber glass waste	56.40 ± 0.6	23.20 ± 0.08	13.60 ± 0.2	5.10 ± 0.02	0.40 ± 0.05	0.60 ± 0.02	0.10 ± 0.01	0.40 ± 0.01	0.20 ± 0.03

(2.5 M NaOH) offers unprecedented opportunities [6].

Low molarity alkaline activation has been extensively studied on waste glass with specific chemistry. Boro-alumino-silicate glass (BSG) powders, from discarded pharmaceutical glass vials, is known to undergo partial dissolution in the activating solution, followed by the evolution of corrosion products upon drying [7]. Part of the dissolved material forms a stable gel, resisting degradation even by immersion in boiling water, and providing a binding phase for adjacent glass particles. In analogy with the zeolite-like gels found in geopolymers (resulting from the dissolution of alumino-silicate feedstock in far more concentrated alkaline solutions) [8], the gel from the alkali activation of BSG may be exploited for dye removal from contaminated waters [6,7]. Sorbents and catalytic destructors with complex 3D architecture may result from the combination of 3D printing, low temperature sintering and low molarity alkaline activation: as shown by Mokhtar et al. [6] exploited the alkaline attack, and the subsequent gel formation, on sintered components, in turn resulting from masked stereolithography.

The present paper aims at offering the integration of low molarity alkaline activation and additive manufacturing, realizing stable glass-based functional scaffolds in the absence of organic binders and sintering treatments. In this framework, the analogy with geopolymers was a fundamental starting point. Highly porous geopolymeric scaffolds are easily manufactured by direct ink writing (DIW), i.e. an extrusion-based additive manufacturing method [9] originally conceived to produce articles from the overlapping of filaments consisting of pastes ('inks'), in turn deriving from the mixing of ceramic particles with organic binders. A key requirement is the non-Newtonian behavior of the inks; the pseudoplasticity enables both easy extrusion from nozzles, in a low viscosity state (at a high shear rate), and stabilization of the shape of the printed part, due to the viscosity increase at a low shear rate [10].

Geopolymeric inks corresponding to suspensions at the early stages of gelation, are typically pseudoplastic; further stabilization of shapes is facilitated by the progression of geopolymerization reactions [11]. We will show that BSG, after activation, offers a similar behavior, even in the absence of any organic additive, to tune the viscosity, giving rise to a real organic-free direct ink writing ('inorganic DIW'). Printed scaffolds were directly usable as filters, without any additional firing step. The stabilization of shapes was supported by mixing with fillers, consisting of porous glass microspheres (PGMs) obtained from waste fiber glass (according to a further process stimulated by the same alkali activation concept) [12]. The cold consolidation, realized by simple drying, is obviously in favor of sustainability, facilitating an extensive reuse of waste glass.

Filtration of organic contaminants is of limited interest once a sorbent is fully saturated. A key to success is the inclusion of photocatalytic phases, such as titanium dioxide (TiO_2) nanoparticles, considered as further fillers. Heterogeneous TiO_2-based photocatalysis is a promising advanced oxidation process for the degradation of various kinds of pollutants in water [13–16]. TiO_2 is recognized as one of the most suitable photocatalysts owing to its inertness, ecological tolerability, low cost, strong oxidizing power, and long-term stability against photo- and chemical corrosion.

It should be noted that TiO_2, due to its relatively wide band gap of 3.2 eV, can be activated just by ultraviolet light, accounting for only 4–5% of the entire solar spectrum [17]. An extensive exploitation of photocatalyst depends on the effectiveness of both capture of molecules and exposition to UV light: we will show that the adopted technology has great potential for the manufacturing of scaffolds with hierarchical porosity, with optimized light exposition offered by complex shapes ('gyroid shaped' scaffolds).

2. Experimental procedure

The chemical compositions of input materials (pharmaceutical and fiber glass), provided in Table 1, were determined by the Bruker Tigers S8 X-ray fluorescence spectrometer (WDXRF).

First, the pharmaceutical glass waste was crushed by ball milling and sieved to obtain a sufficient amount of glass powder (precursor) with a particle size below 40 μm. Then the prepared fine glass powder was mixed with 20 wt% TiO_2 (21 nm, Evonik Degussa GmbH, Germany). The prepared precursor (glass powder with TiO_2) was mixed at 800 rpm for 2 h and then at 1600 rpm for 1 h into an aqueous solution containing 2.5 M NaOH (reagent grade, Sigma-Aldrich, UK) to obtain a homogeneous aggregate-free mixture. The solid loading in the alkaline solution was 65 wt%. After alkaline activation, the obtained suspension/ink was ready for DIW printing process.

Second, the fiber glass waste was crushed, sieved through a 40 μm analytical sieve, alkali activated in 9 M KOH solution, following the process reported in a previous study [12]. The gel, hardened at 75 °C, was then crushed and sieved through analytical sieves to obtain a fraction of 40–80 μm in size. These crushed fragments were projected against an oxygen-methane torch, by means of a vacuum powder feeder (oxygen used as carrier gas). Droplets of molten glass were transformed into porous glass microspheres (PGMs), quenched in deionized water. The PGMs were separated by microfiltration through a ceramic filter with a pore size < 0.3 μm.

The fabricated PGMs were added into the pre-prepared homogenous ink containing pharmaceutical glass powder and TiO_2 powder at the weight fraction of 20 and 30 wt% by mixing at 1000 rpm for 30 min. The ink was loaded in the DIW device after complete mixing. Printing was performed using a commercial DIW printer (Delta Wasp 206 Turbo, Massa Lombarda, Italy), and extruder (PowerWasp Evo, Wasp, Massa Lombarda, Italy). The printer was equipped with a pressurized container and an endless screw, which allows the extrusion of highly viscous pastes. A conical nozzle (diameter of 810 μm, Nordson EFD, Westlake, OH, USA) was used to extrude a filament with a final diameter of approximately 800 μm using compressed air.

The filaments were deposited on a glass substrate, covered by a plastic sheet for easy removal of the green scaffolds. A lattice and a gyroid with the size of $20 \times 20 \times 5$ and $30 \times 30 \times 5$ mm^3 were printed. The radius and the height of the filter were 13.5 and 5 mm respectively, with 1 mm spanning length between the centers of two contiguous filaments. The z-axis displacement (i.e. the layer thickness) was nearly 750 μm, which led to a certain overlapping and increased the adhesion between the scaffold layers. After printing, the samples were left to dry and solidify at ambient temperature for 24 h. Afterwards, the samples were usable for physical, mechanical, and photocatalytic testing.

The apparent and true density were measured by helium pycnometry (Anton Paar, Ultrapyc 3000), using bulk or finely crushed samples, respectively. A stainless-steel ball (1.0725 g) was used as a calibration standard, with 7 readings for calibration. The density values were used to compute the amounts of open and closed porosity. The compressive strength of the dried objects was measured using a universal testing machine (Quasar 25, Galdabini S.p.a., Cardano al Campo, Italy),

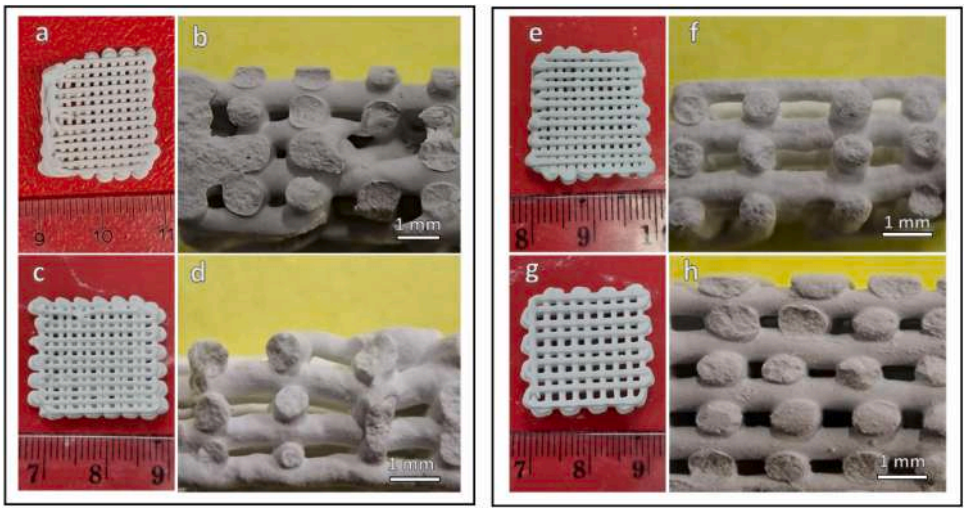

Fig. 1. Preliminary extrusion experiments: a,b) ink from activated BSG; c,d) ink with TiO_2 addition; e,f) ink with TiO_2 + 20% PGMs; e,f) ink with TiO_2 + 30% PGMs.

operating at a crosshead speed of 0.5 mm/min).

The specific surface area was measured by N_2 physisorption at − 196 °C (ASAP 2010, Micromeritics, Norcross, GA, USA). The samples were degassed at 150 °C, and the specific surface area was calculated in the relative pressure (p/p_0) range between 0.05 and 0.30 by applying the Brunauer–Emmett–Teller (BET) multipoint method.

The printed samples were examined by XRD before and after activation using the powder diffractometer, Panalytical Empyrean, with Bragg-Brentano geometry, at an accelerating voltage of 45 kV, using Cu Kα radiation with λ = 1.545 Å. Diffraction patterns were collected in the 2θ range of 10–70°. The absorption infrared spectra of glass particles were measured using FT/IR (JASCO, USA). The microstructure of the printed pharmaceutical glass was examined using a scanning electron microscope (SEM; Jeol JSM 7600 F, Tokyo, Japan), with 1.2 kV acceleration voltage.

The fabricated 3D glass composite with the different formulations BSG+TiO_2, BSG+TiO_2 + 20PGMs and BSG+TiO_2 + 30PGMs denote pharmaceutical glass with added titania, pharmaceutical glass with added titania and 20 wt% PGMs and pharmaceutical glass with added titania and 30 wt% PGMs, respectively. Samples of the same weight (0.3 g) were used for a photo-degradation test consisting of immersion of the structure for 90 min into 50 mL of methylene blue solution (initial concentration of 50 mg/L), irradiated by UV (λ = 366 nm, power = 125 W, Helios Italquartz S.R.L., Milan, Italy). The residual concentration of the dye was determined by measuring the absorbance of the solution at 664 nm (λ_{max}) using a UV–VIS spectrophotometer (Jasco V-650, Easton, MD, USA).

3. Results and discussion

The pseudo-plasticity of geopolymer-yielding slurries is known as the fundamental background of highly porous foams manufactured by ‘gel casting’, consisting of intensive mechanical stirring with the help of a surfactant. Air bubbles are first incorporated in a low viscosity state (at the high shear rate, upon intensive mechanical stirring) and then ‘frozen’ by a sudden increase of viscosity (at the low shear rate, when stirring stops) [18]. The exploitation in direct ink writing can be seen as a logical extension [19].

Several studies demonstrated that pseudoplastic slurries may be achieved well beyond formulations leading to geopolymers, i.e. with gelation phenomena not corresponding to the development of a three-dimensional alumino-silicate network (‘zeolite-like gel’) [20,21]. Rincón et al. [22], for example, prepared glass foams by viscous flow sintering of ‘green’ foams formed at nearly room temperature by intensive mechanical stirring of aqueous suspensions of fine glass powders (solid loading of 65 wt%), subjected to a ‘weak’ alkali activation (2.5 M KOH).

Soda-lime glass, upon alkali activation, does not yield a zeolite-like gel, but it is prone to the formation of calcium silicate hydrates (C-S-H), i.e. compounds with a layered structure and limited chemical stability (layers featuring strong chemical bonds are mutually connected by weak bonds) [23]. On the contrary, nearly Ca-free pharmaceutical glass, with a relatively high Al_2O_3 content, under the conditions of ‘weak’ activation undergoes gelation by the formation of strong Si-O-Si, Si-O-Al and Si-O-B bonds. Solid compacts from dried suspensions are not degraded by immersion in boiling water, with the exception of the dissolution of secondary phases, such as hydrated alkali carbonates [7].

The analogy with geopolymers, i.e. yielding a product with strong chemical bonds at a nearly room temperature (cold consolidation), constituted the reference for the present work. BSG suspensions, upon activation with 2.5 M NaOH, were not left in containers for 24 h at 75 °C in ’static’ mode (following the preliminary dissolution stage) for complete hardening. Instead, they were utilized during the early stages of gelation, after a ’curing’ stage of 3 h at 25 °C.

Fig. 1 illustrates that this choice led to printable inks: extruded filaments could be easily overlapped, forming lattice structures. Since gelation was not complete, the viscous flow after extrusion was not controlled: despite the successful stacking of filaments (Fig. 1a) the scaffolds from pure BSG exhibited a significant sagging (Fig. 1b), accompanied by the collapse of transverse porosity. Ideally, this could be avoided by prolonging the curing step, promoting gelation. However, the addition of the photocatalytic additive (TiO_2 nanoparticles) proved to be useful also in limiting the flow of pastes after extrusion. The increase of the viscosity of suspensions, as the result of addition of nanoparticles, is well known [24]: despite the reduction of the amount of activated glass that contributed to hardening, the overlapping of filaments was still satisfactory (Fig. 1c); the increase of viscosity due to the addition of nanoparticles limited the sagging (Fig. 1d).

Further optimization was achieved by the inclusion of a lightweight filler, also prepared from waste glass, i.e. fiber glass-derived porous glass microspheres [12]. Despite the reduction of the amount of material undergoing gelation, the addition of PGMs did not compromise the stacking of filaments (Fig. 1e,g), but suppressed the sagging (Fig. 1f,h), by reducing the gravity-induced deformation.

The optimized ink, comprising both TiO_2 and PGMs, was used in a second series of experiments, also for more complex shapes. Fig. 2a-d outlines the progressive printing of a gyroid structure based on BSG+TiO_2 + 30PGMs ink, starting from the first deposited filament

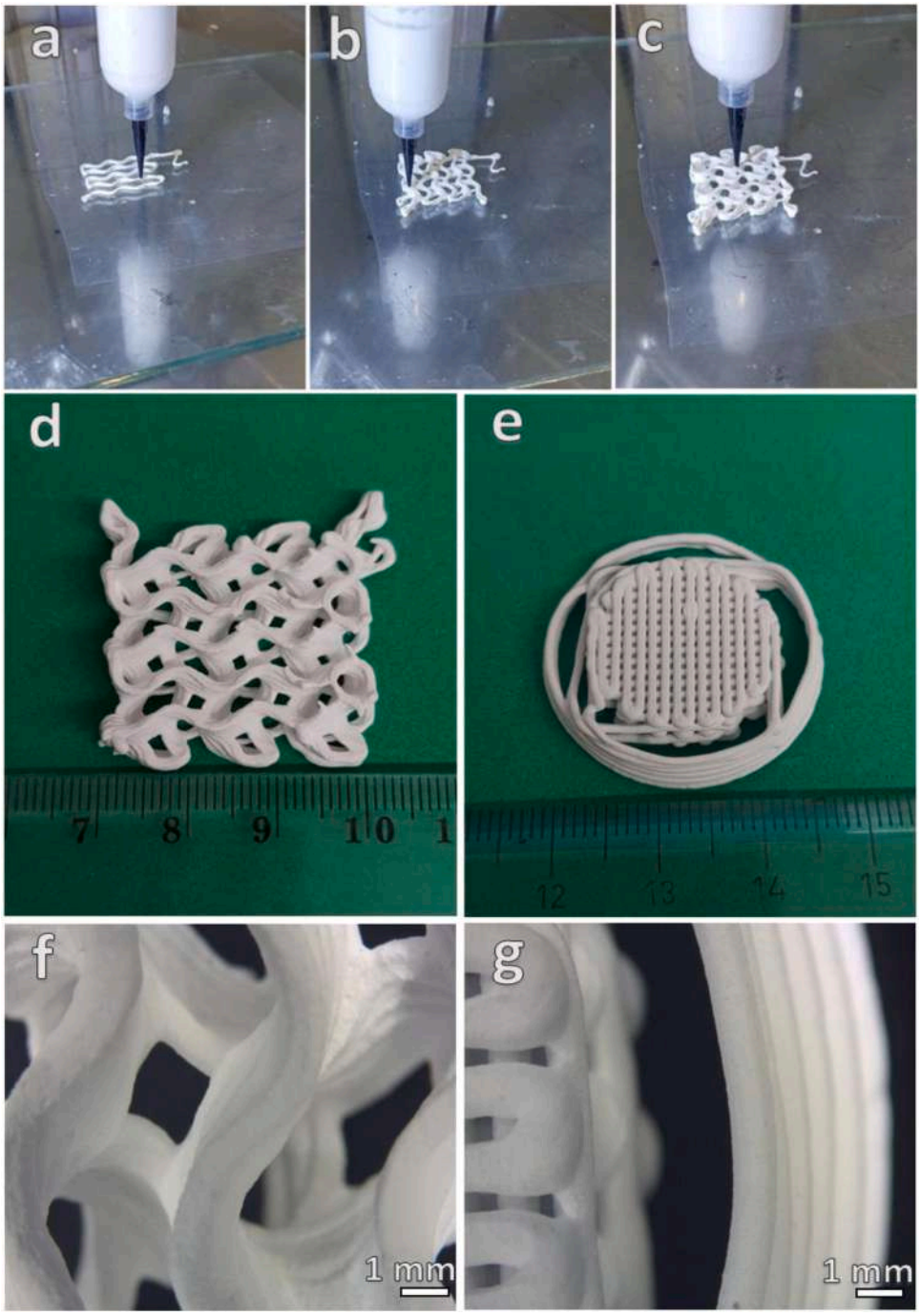

Fig. 2. Refined printing experiments: a-c) printing operation; d,f) details of gyroid structure; e,g) details of 'filament-filter' structure.

Table 2
Physical and mechanical properties of the printed glass-based composites.

Samples	ρ_{geom} (g/cm^3)	ρ_{app} (g/cm^3)	ρ_{true} (g/cm^3)	Total porosity *P* (%)	Open porosity *OP* (%)	Closed porosity *CP* (%)	Compressive strength (MPa)	Surface area (m^2/g)
BSG +TiO_2	0.97 ± 0.01	2.73 ± 0.06	2.86 ± 0.06	65 ± 1	64 ± 1	1 ± 1	0.3 ± 0.1	24.7
BSG+TiO_2 + 20PGMs	0.91 ± 0.01	2.70 ± 0.04	2.81 ± 0.04	67 ± 1	66 ± 1	1 ± 1	1.2 ± 0.2	31.8
BSG+TiO_2 + 30PGMs	0.77 ± 0.02	2.71 ± 0.03	2.77 ± 0.03	72 ± 1	71 ± 1	1 ± 1	1.5 ± 0.2	40.3

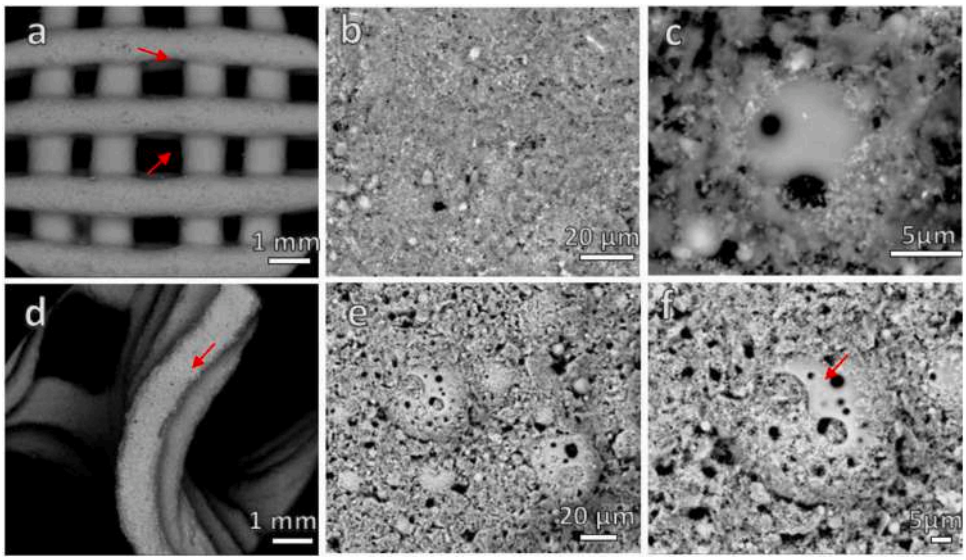

Fig. 3. Scanning electron microscope images of printed composite by DIW based BSG+TiO_2 + 30PGMs (a, b and c) lattice structure (d, e and f) gyroid structure.

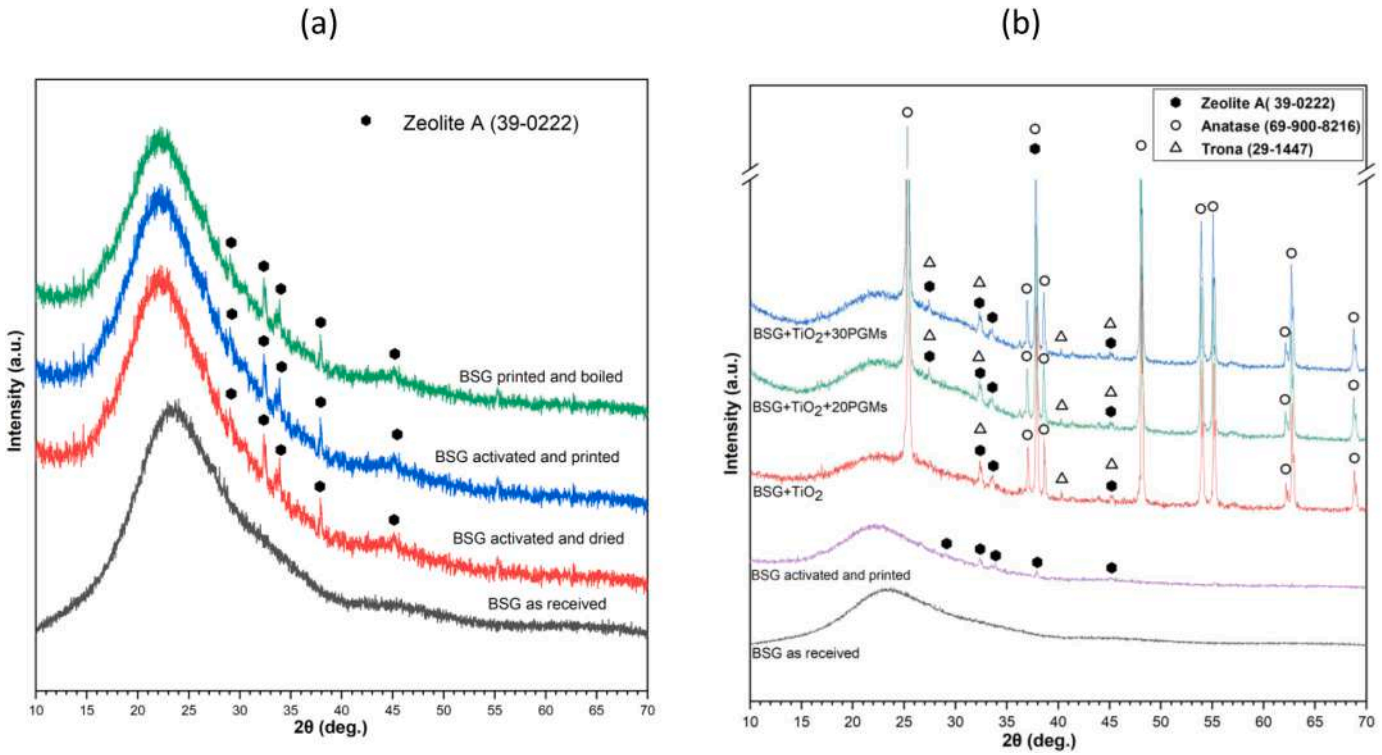

Fig. 4. (a) XRD of BSG: as received, activated and dried, activated and printed and printed and boiled, (b) XRD of BSG: activated and printed, BSG+TiO_2 printed, BSG+TiO_2 + 20PGMs printed and BSG+TiO_2 + 30PGMs printed.

layer (Fig. 2a), going through the second layer (Fig. 2b) up to nearly complete structure (Fig. 2c). Besides gyroids (Fig. 2d), the ink allowed also for easy fabrication of other shapes, such as the 'filament-filter' structure, shown in Fig. 2e. Additional details on the successful stacking, with only limited deformations, are shown in the optical stereomicroscopy images in Fig. 2f,g.

The physical and mechanical properties of the printed objects after drying are shown in Table 2. By incorporating PGMs into the activated glass ink, the porosity increased from 65% to 72% and was nearly completely open. The specific surface area increased from approximately 25 to 40 m^2/g. The relatively high surface area is attributed to the incorporation of PGMs, in addition to the outcome products of alkali activation and the presence of titania nanoparticles. The compressive strength of the printed scaffolds increased significantly, from 0.3 to 1.5 MPa. For highly porous bodies (e.g. porosity above 70%), a fundamental reference in the analysis of the strength-density correlation is provided by the Gibson and Ashby [25] model, according to which the compressive strength of an open-celled porous body is ruled by (Eq. 1):

$$\sigma_c \approx 0.2 \bullet \sigma_{bend} \bullet \rho_{rel}^{1.5} \quad (1)$$

where ρ_{rel} is the relative density ($\rho_{rel} = 1 - P/100$), P is the total porosity and σ_{bend} is the bending strength of the solid phase in the struts. The

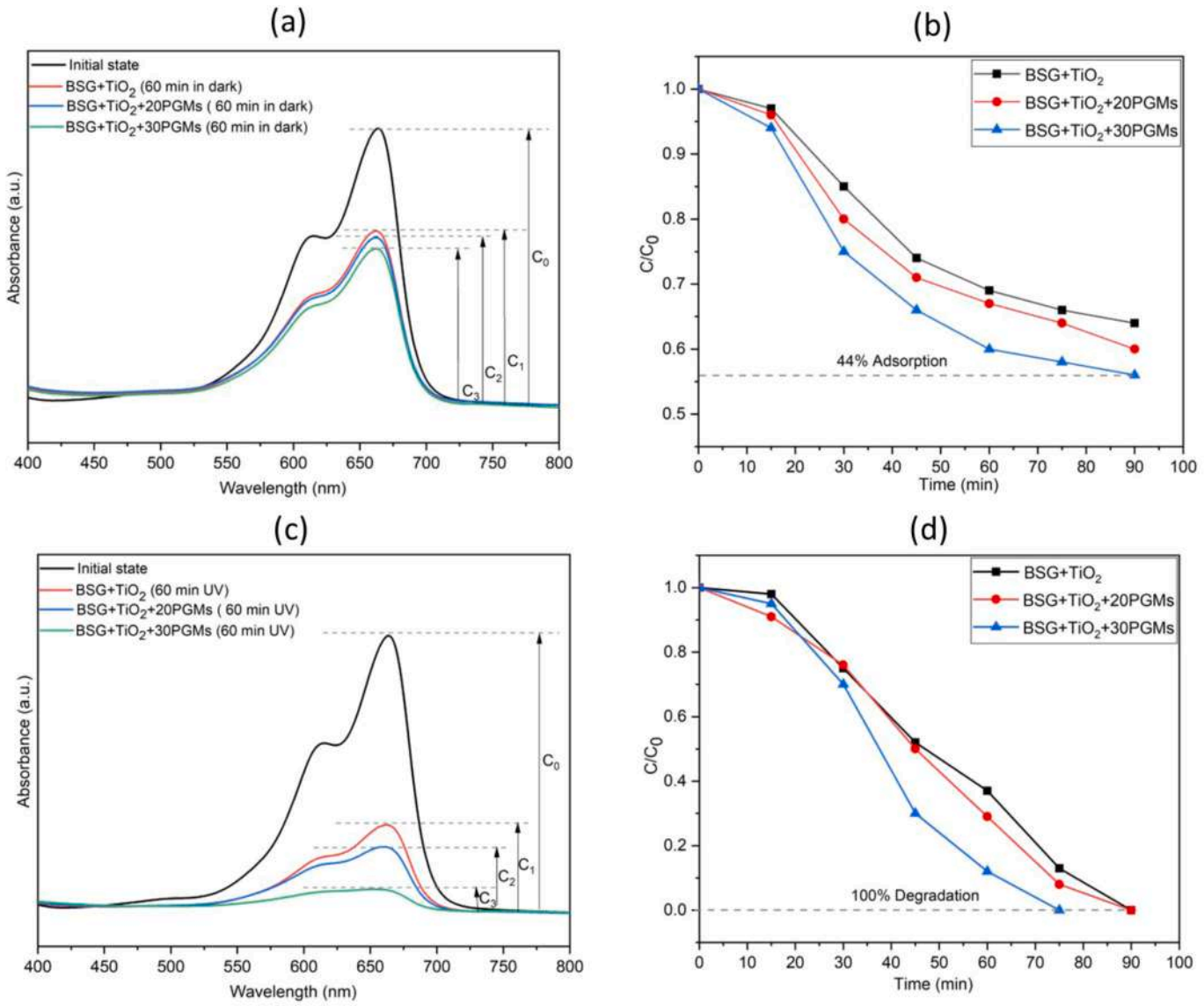

Fig. 5. (a) Absorption spectra of the methylene blue solution in the initial state and after 60 min in contact with printed glass-based composites in dark (b), evolution of the relative concentration of methylene blue with increasing the adsorption time (c) Absorption spectra of the methylene blue solution in the initial state and after 60 min in contact with printed glass-based composites under UV exposure (d), evolution of the relative concentration of methylene blue with increasing UV exposition time.

highest compressive strength measured for the sample BSG+TiO_2 + 30PGMs, considering the relative density (ρ_{rel}=1–0.72 =0.28), is consistent with a bending strength of the material in the strut of approximately 50 MPa. Such value is impressive: despite the absence of any firing step the value is close to the bending strength of solid glass (~70–80 MPa [26]). The cold consolidation process thus promoted the formation of strong bonds between glass particles. In particular, PGMs were likely integrated into the cementitious matrix formed by activated BSG.

Fig. 3. reports some details observed by SEM. Overlapping filaments created wide contact zones (marked by arrows in Fig. 3a,d), and their interpenetration likely minimized stress concentrations. PGMs were homogeneously dispersed (Fig. 3c,d) and firmly embedded in the matrix (Fig. 3e,f). The matrix even partially penetrated the pore openings of PGMs (see arrow in Fig. 3f). (Fig. 3c,d) embedding them firmly in the matrix.

The changes in the nature of the gel related to the activation and titania addition were provided by X-ray powder diffraction analysis (see Fig. 4a and Fig. 4b). The activation with 2.5 M NaOH solution led to the formation of zeolite A ($Na_{12}((AlO_2)_{12}(SiO2)_{12})\cdot 27\ H_2O$), (Fig. 4a), in accordance with previous investigations on foams [27] after activation with NaOH. No differences in diffraction patterns are detected between the dried and printed activated BSG. The zeolite phase was accompanied by a newly formed amorphous gel, as suggested by the shift of the 'amorphous halo' compared to the as-received glass [7], as shown in Fig. 4a. The stability of 3D-printed composites concerning thermal treatment is guaranteed as long as the zeolite phase remained intact even after the boiling test (immersing the 3D printed composites in boiling water for 20 min).

Fig. 4b documents the mixture of phases upon adding titania into the printed composites BSG+TiO_2, BSG+TiO_2 + 20PGMs, and BSG+TiO_2 + 30PGMs. Activated glass suspensions with added titania yielded materials featuring anatase, zeolite A, and trona (sodium carbonate hydrate, $Na_3(CO_3)(HCO_3)\cdot 2\ H_2O$).

The data in Table 2 and Fig. 3 reveal that the printed samples contained hierarchical porosity. The overall measured porosity is well above the value resulting from the stacking of filaments. Besides macroporosity, from printing, porosity was expressed by nano-sized voids

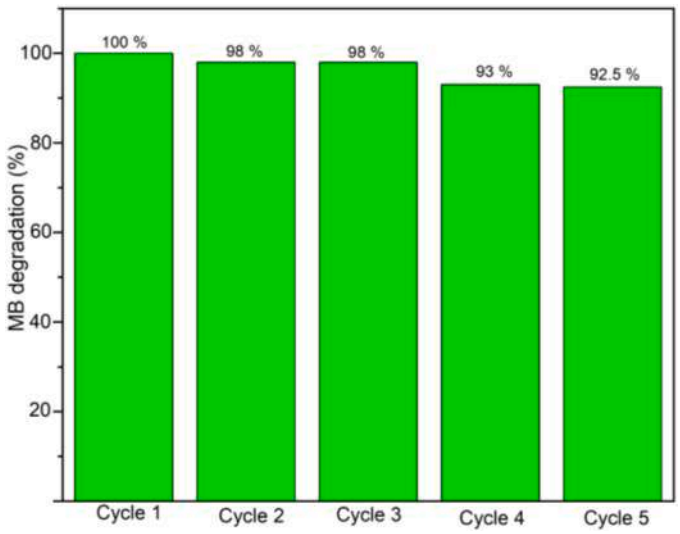

Fig. 6. Evolution of methylene blue degradation (%) with the number of cycles.

left between adjacent particles or inside the microspheres and in the binding gel. In other words, the increased porosity of these materials also leads to enhanced ultraviolet (UV) exposure within the structure and consequently the adsorption of organic molecules. Fig. 5 confirms such assumption, with photocatalytic effects maximized with the BSG+TiO_2 + 30PGMs sample.

Fig. 5a presents the absorption spectrum of a methylene blue solution (50 mg/L) in deionized water. The absorbance peak at 664 nm serves as the reference for the determination of initial dye concentration (C_0). The adsorption of methylene blue is discerned through the reduction in absorbance resulting from immersing the samples in a methylene blue solution in the absence of light. Fig. 5b illustrates that the maximum adsorption efficiency, achieved within 90 min, reached 44% for the sample denoted as BSG+TiO_2 + 30PGMs. This enhancement in adsorption can be ascribed to its superior porosity and larger surface area, as outlined in Table 2, compared to other samples. The observed adsorption efficiency holds significance as it can contribute to augmenting the photodegradation performance of the samples, which constitutes the primary objective of this current investigation. It is worth noting that adsorption represents the initial step in the photodegradation process.

Fig. 5c presents the absorption spectra of the methylene blue solution in contact with printed glass-based composites under UV exposure. The

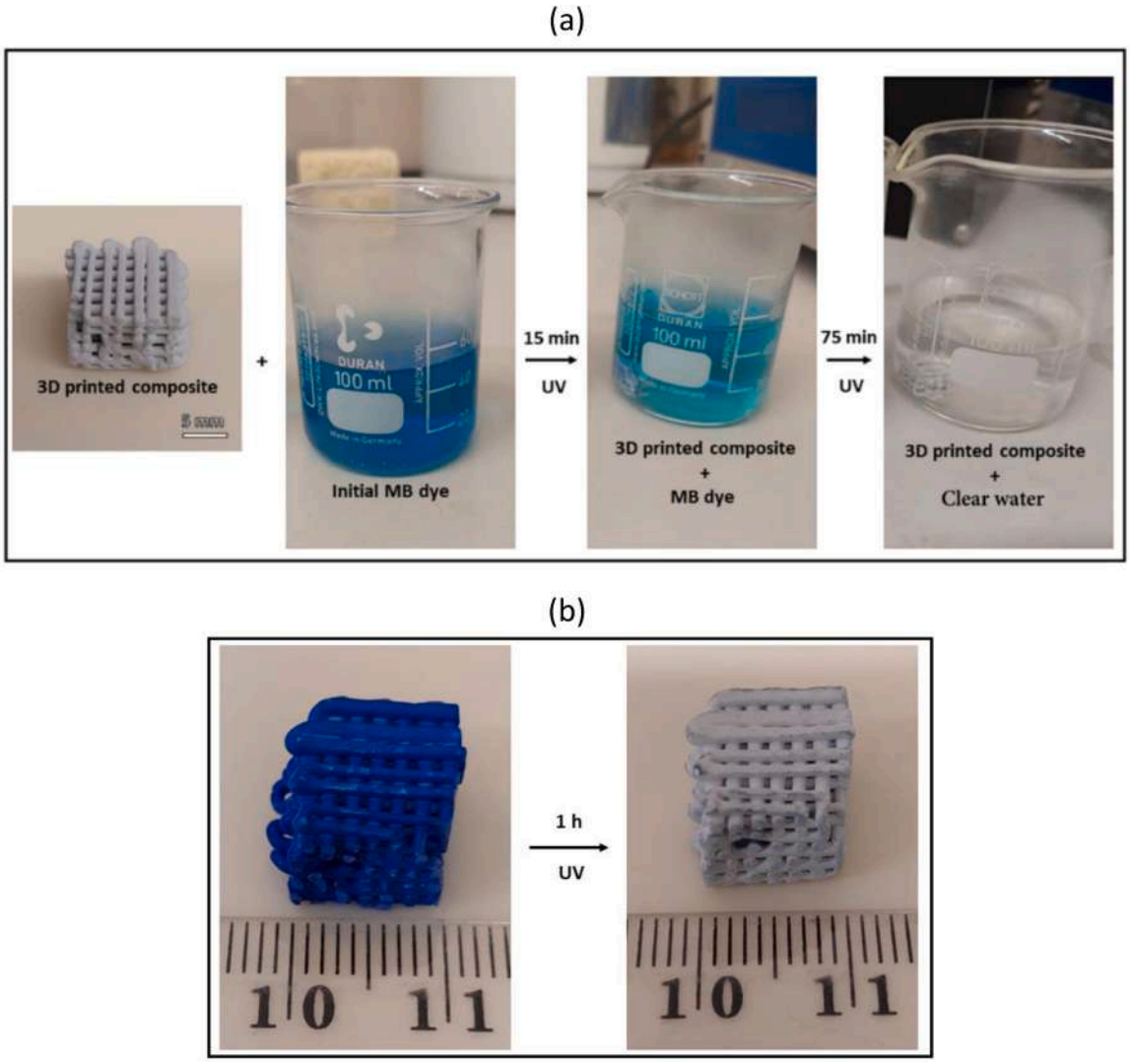

Fig. 7. (a) schematic diagram of photodegradation of methylene blue by 3D printed composite, (b) cleaning the adsorbed methylene blue on the 3D printed composite by UV light.

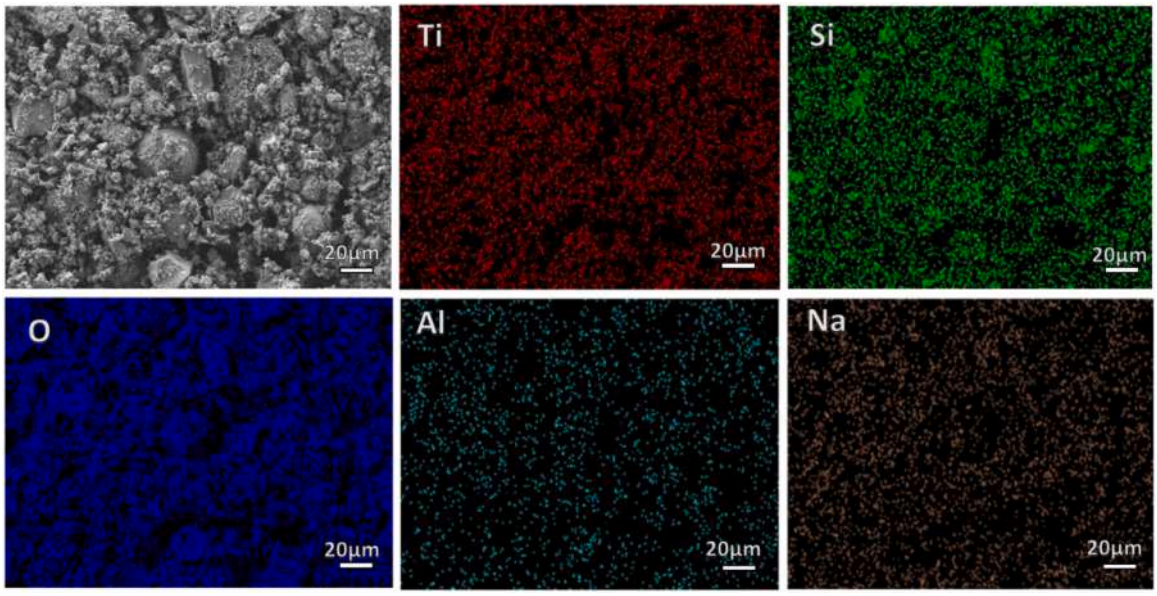

Fig. 8. Map EDS of the surface of the reused 3D printed composite after 5 cycles.

sensitivity to UV degradation of the specific organic species is inferred from the decrease in absorbance after 60 min irradiation. It can be noted that the presence of TiO_2 leads to a reduction of ~62% in the intensity of the absorbance peak ($C/C_0 = 0.38$ for BSG+TiO_2 scaffold). More porous scaffolds, containing PGMs, maximized the reduction of the intensity (70% and 88% for BSG+TiO_2 +20PGMs and BSG+TiO_2 +30PGMs respectively).

Longer exposition times (Fig. 5d), up to 75 min, resulted in a nearly undetectable signal at 664 nm and corresponded to the complete removal of the methylene blue dye from the solution for the samples BSG+TiO_2 + 30PGMs. Samples BSG+TiO_2 and BSG+TiO_2 + 20PGMs achieved 100% degradation after a longer exposition (Fig. 5d).

3.1. Regeneration and reusability

Recovery and reusability are crucial parameters for selecting inexpensive and viable catalysts for pilot-scale remediation systems. To verify the recyclability of the printed scaffolds, BSG+TiO_2 + 30PGMs samples were subjected to 5 consecutive degradation cycles, to evaluate the preservation of their photodegradation capacity. The degradation performance of methylene blue after 5 cycles was nearly 93%, (Fig. 6). After each cycle, the scaffolds were exposed to a UV lamp for 1 h and reused.

The slight decrease in the degradation efficiency over subsequent cycles can be explained by considering a couple of key factors. Firstly, there may be a slight loss of material during the recovery step when the samples are physically removed from and re-immersed into the methylene blue solution. This can result in a reduced dosage of the catalyst in each subsequent cycle, leading to lower surface activity and overall lower performance [28]. Secondly, the gradual decrease in active sites may occur after each cycle due to the clogging of the pores by the adsorbed methylene blue [29]. As the cycles progress, the pores within the catalyst may become partially blocked, reducing their availability for adsorption and subsequent photodegradation processes. It is important to note that, in general, several cycles can be conducted using the same material with almost the same pollutant degradation efficacy, demonstrating the potential for material durability and continued effectiveness over multiple cycles.

Fig. 7a shows the schematic diagram of the photodegradation of methylene blue by 3D printed composite, starting from immersing the 3D printed composite into the solution with the initial concentration of

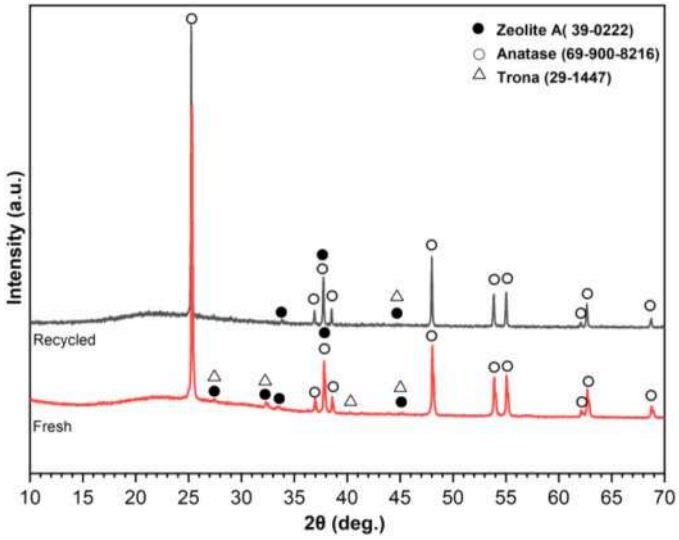

Fig. 9. XRD of the fresh and recycled 3D printed composite.

methylene blue 50 mg/L. The methylene blue degraded completely under UV light exposure (75 min) yielding clear water. The 3D-printed composite can be reused several times, degrading adsorbed dye by the exposure to UV light. To demonstrate the high efficiency of the cleaning process using 3D printed composites, the sample is immersed in a methylene blue solution for 24 h (to allow for adsorption without UV exposure). Subsequently, the sample is exposed to UV light for 1 h to clean the adsorbed methylene blue. The successful cleaning process of the 3D-printed composite is illustrated in Fig. 7b.

3.1.1. Characterization of the regenerated materials

The surface of the reused 3D printed composite was investigated by EDS mapping (Fig. 8). The EDS maps confirmed the presence of characteristic elements of Ti, Si, Al, and Na on the surface of the printed composites. The results support the XRD data, which documented the presence of anatase and zeolite diffraction maxima (Fig. 9).

The uptake and photodegradation of methylene blue by regenerated and re-used 3D-printed composites remained substantial, as shown in Fig. 6. Notably, the analysis of side views of the reused 3D-printed

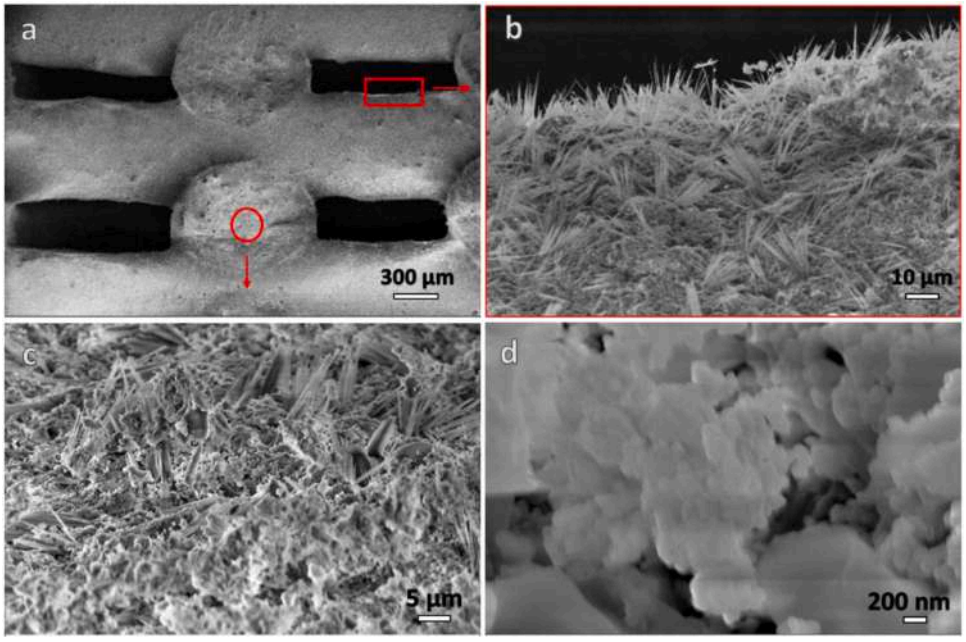

Fig. 10. Scanning electron microscope images of the reused 3D printed composite after 5 cycles (a) the side view, (b) higher magnification of the area in red rectangle, (c) cross-section of the filament, and (d) higher magnification of the cross-section of the filament.

Table 3
A comparison of photocatalytic materials with their degradation efficiency of methylene blue dye.

Materials	Initial concentration mg/L	Dose of photocatalysts g	Degradation efficiency (%)	Time of degradation (min)	Ref
Fe_2O_3/TiO_2 composite ceramic	25	2	83	240	[31]
TiO_2 nano composite	6	0.5	86	60	[32]
TiO_2	25	2	90	120	[33]
Fe_3O_4/AC/TiO_2 Nano-Catalyst	100	0.1	98	60	[34]
Na-TiO_2 nano tube	10	0.5	98.5	60	[35]
TiO_2-Polymeric Substrates	4	0.1	100	110	[36]
This work	50	0.3	100	75	

composite (Fig. 10a) demonstrated the absence of any sagging in the z-direction, despite the considerable distance between parallel filaments. Sagging is a common issue encountered in 3D printing, especially when there are significant gaps or unsupported overhangs between the printed layers. This phenomenon occurs due to the weight of the upper layers exerting pressure on the lower ones during printing, leading to deformation[30]. However, the absence of sagging in the reused composite indicates its structural integrity and highlights its potential for reliable applications in 3D printing processes. A higher magnification imaging of the place marked by the red rectangle (Fig. 10b) revealed formation of a rough surface of the mixed zeolite and anatase phases, which could be considered beneficial for the dye adsorption. Fig. 10c shows a high magnification image of the cross-section of the filament (marked by the red circle in Fig. 10a), revealing rough texture of mixed crystals. A higher magnification of the spot marked by the red circle in Fig. 10c reveals the formation of nanocrystals (see Fig. 10d), which have a crucial role in increasing the number of active sites for adsorption and subsequently the photodegradation process [6,7].

3.2. Comparison of photocatalysts

The efficiency of various photocatalytic materials designed for the degradation of methylene blue dye is compared in Table 3. However, the sample dose varies significantly, ranging from 0.1 to 2 g, and the initial dye concentration varies from 4 to 100 mg/L. Our photocatalyst compares favorably with other studies, exhibiting a faster degradation rate and requiring a moderate sample dose. The successful application in dye destruction, coupled with sustainable processing (no organic additives, no high-temperature treatment for debinding and sintering), make the developed scaffold a particularly promising example of upcycling of waste glass.

3.3. Economic advantage of the proposed strategy

To highlight the economic advantage for the fabricated photocatalysts, we need to consider various factors that can validate the proposed strategy compared to existing literature, as follows:

a) Raw material: the use of waste glass as a raw material is a significant advantage as it reduces the cost of acquiring new materials compared to other photocatalysts that may rely on more expensive or resource-intensive materials.
b) Fabrication process: the fabrication process, which utilizes direct ink writing without any organic additives, can reduce production costs and evaluate the cost savings compared to traditional methods.
c) Energy consumption: since there is no sintering or high-temperature treatment involved, there are energy savings in the production process compared to other traditional methods that require high-temperature processing.
d) Performance and regeneration: considering the cost savings associated with not needing to frequently replace the photocatalysts due to their effective regeneration, this approach is highly economical.

e) Reusability and maintenance: assessing the ease of reusing the samples by exposing them to UV light can reduce the need for frequent replacements.
f) Environmental impact: the study focuses on the utilization of pharmaceutical glass waste and fiber glass waste to create functional materials. This upcycling approach reduces the need for disposal of these waste materials in landfills, potentially lowering environmental pollution. Moreover, the application of 3D-printed composites for the photodegradation of methylene blue suggests a potential positive environmental impact in terms of water treatment and pollution control.

4. Conclusions

In this work, pharmaceutical glass waste (BSG) was successfully converted into photocatalytic scaffolds by a cold consolidation process (not including any firing step), using direct ink writing of suspensions of fine powders in an alkaline solution. The main conclusions are as follows:

- The inclusion of titania nanoparticles (20 wt%) and porous glass microspheres (20–30 wt%) enables the printing of regular scaffolds, with only limited deformation;
- After alkali activation, BSG yields stable gels that form strong bonds between adjacent particles; this is not compromised by the inclusion of additives;
- The uniformity and the strong adhesion between individual components enabled the achievement of a high strength-to-density ratio (compressive strength of 1.5 MPa, with the porosity exceeding 70%);
- The reaction rate of DIW-processed scaffolds for achieving 100% degradation of methylene blue is 75 min, which compares favorably with other reported TiO_2-based composites, ranging from 90 to 240 min. Furthermore, the samples can be re-used for five cycles without experiencing a significant loss of efficiency;

This study creates new pathways for upcycling and functionalizing waste glass and its use in environmental applications.

CRediT authorship contribution statement

Mokhtar Mahmoud, Data curation; Formal analysis; Investigation; Validation; Visualization; Roles/Writing - original draft, Jozef Kraxner, Project administration; Resources; Supervision; Writing - review & editing Akansha Mehta, Conceptualization; Data curation; Investigation; Supervision; Hamada Elsayed, Conceptualization; Data curation; Formal analysis; Investigation; Methodology; Supervision; Writing - review & editing, Dusan Galusek,Funding acquisition; Project administration; Resources; Supervision; Validation; Writing - review & editing, Enrico Bernardo, Conceptualization; Funding acquisition; Methodology; Project administration; Resources; Supervision; Visualization; Writing - review & editing.

Declaration of Competing Interest

The authors declare **no conflict of interest**.

Acknowledgments

This paper is a part of the dissemination activities of the project “FunGlass” (Centre for Functional and Surface Functionalized Glass). This project has received funding from the European Unionś Horizon 2020 research and innovation program under grant agreement no. 739566. Enrico Bernardo acknowledges the additional funding from the University of Padova (Dept. of Industrial Engineering), in the framework of the “SusPIRe” (Sustainable porous ceramics from inorganic residues, BIRD202134). Hamada Elsayed acknowledges the support of national project MUR PON R&I 2014-2021. The authors also gratefully acknowledge the financial support from the Slovak Grant Agency of Ministry of Education, Science, Research and Sport, VEGA No 1/0456/20.

References

[1] A. Nommeots-Nomm, P.D. Lee, J.R. Jones, Direct ink writing of highly bioactive glasses, J. Eur. Ceram. Soc. 38 (3) (2018) 837–844, https://doi.org/10.1016/j.jeurceramsoc.2017.08.006.
[2] Y. Peng, Y. Zhang, Preparation of highly dispersible glass frit powders and its application in ink-jet printing ink, J. Eur. Ceram. Soc. 40 (9) (2020) 3489–3493, https://doi.org/10.1016/j.jeurceramsoc.2020.03.058.
[3] T.I. Kwinda, B. Oberleiter, K. Fischer, I. Thomas, A. Schulze, D. Enke, S. Koppka, Evaluating the photocatalytic activity of 14.6TiO_2–7Na_2O–23B_2O_3-55.4SiO_2 (mol.-%) glass based porous catalysts after selective laser sintering and conventional shaping, Ceram. Int. 48 (22) (2022) 34064–34074, https://doi.org/10.1016/j.ceramint.2022.07.355.
[4] A. Dasan, P. Ozog, J. Kraxner, H. Elsayed, E. Colusso, L. Grigolato, G. Savio, D. Galusek, E. Bernardo, Up-Cycling of LCD glass by additive manufacturing of porous translucent glass scaffolds, Materials 14 (17) (2021), https://doi.org/10.3390/ma14175083.
[5] E. Bernardo, R. Cedro, M. Florean, S. Hreglich, Reutilization and stabilization of wastes by the production of glass foams, Ceram. Int. 33 (6) (2007) 963–968, https://doi.org/10.1016/j.ceramint.2006.02.010.
[6] M. Mahmoud, J. Kraxner, H. Elsayed, D. Galusek, E. Bernardo, Advanced dye sorbents from combined stereolithography 3D printing and alkali activation of pharmaceutical glass waste, Materials 15 (2022) 6823, https://doi.org/10.3390/ma15196823.
[7] A. Mehta, K. Karbouche, J. Kraxner, H. Elsayed, D. Galusek, E. Bernardo, Upcycling of pharmaceutical glass into highly porous ceramics: from foams to membranes, Materials 15 (11) (2022), https://doi.org/10.3390/ma15113784.
[8] Y. Luo, Z. Jiang, D. Wang, Y. Lv, C. Gao, G. Xue, Effects of alkaline activators on pore structure and mechanical properties of ultrafine metakaolin geopolymers cured at room temperature, Constr. Build. Mater. 361 (2022), 129678, https://doi.org/10.1016/j.conbuildmat.2022.129678.
[9] A. Shahzad, I. Lazoglu, Direct ink writing (DIW) of structural and functional ceramics: recent achievements and future challenges, Compos. B: Eng. 225 (2021), 109249, https://doi.org/10.1016/j.compositesb.2021.109249.
[10] K. Huang, H. Elsayed, G. Franchin, P. Colombo, Embedded direct ink writing of freeform ceramic components, Appl. Mater. Today 23 (2021), 101005, https://doi.org/10.1016/j.apmt.2021.101005.
[11] H. Jin, Y. Zhang, X. Zhang, M. Chang, C. Li, X. Lu, Q. Wang, 3D printed geopolymer adsorption sieve for removal of methylene blue and adsorption mechanism, Colloids Surf. A 648 (2022), 129235, https://doi.org/10.1016/j.colsurfa.2022.129235.
[12] M. Mahmoud, J. Kraxner, H. Kaňková, M. Hujová, S. Chen, D. Galusek, E. Bernardo, Porous glass microspheres from alkali-activated fiber glass waste, Materials 15 (3) (2022) 1043, https://doi.org/10.3390/ma15031043.
[13] C.L. Heredia, dL. Sham, lM. Farfán-Torres, Tartrazine degradation by supported TiO_2on magnetic particles, Matér. (Rio De. Jan.) 20 (3) (2015) 668–675, https://doi.org/10.1590/s1517-707620150003.0069.
[14] M. Pelaez, N.T. Nolan, S.C. Pillai, M.K. Seery, P. Falaras, A.G. Kontos, P.S. M. Dunlop, J.W.J. Hamilton, J.A. Byrne, K. O'Shea, M.H. Entezari, D.D. Dionysiou, A review on the visible light active titanium dioxide photocatalysts for environmental applications, Appl. Catal. B. 125 (2012) 331–349, https://doi.org/10.1016/j.apcatb.2012.05.036.
[15] A. Manassero, M.L. Satuf, O.M. Alfano, Photocatalytic degradation of an emerging pollutant by TiO_2-coated glass rings: a kinetic study, Environ. Sci. Pollut. Res Int 24 (7) (2017) 6031–6039, https://doi.org/10.1007/s11356-016-6855-2.
[16] A. Fujishima, X. Zhang, D. Tryk, TiO_2 photocatalysis and related surface phenomena, Surf. Sci. Rep. 63 (12) (2008) 515–582, https://doi.org/10.1016/j.surfrep.2008.10.001.
[17] G. Wang, L. Xu, J. Zhang, T. Yin, D. Han, Enhanced photocatalytic activity of powders (P25) via calcination treatment, Int. J. Photo 2012 (2012) 1–9, https://doi.org/10.1155/2012/265760.
[18] J. Zhu, J. Yu, Y. Wu, Y. Chao, P. Wu, L. Lu, L. Chen, J. He, W. Zhu, Engineering 3D-printed aqueous colloidal ceramic slurry for direct ink writing, Green. Chem. Eng. (2022), https://doi.org/10.1016/j.gce.2022.04.005.
[19] L. del-Mazo-Barbara, M.P. Ginebra, Rheological characterisation of ceramic inks for 3D direct ink writing: A review, J. Eur. Ceram. Soc. 41 (16) (2021) 18–33, https://doi.org/10.1016/j.jeurceramsoc.2021.08.031.
[20] S.H. Hajiabadi, M. Khalifeh, R. van Noort, P.H. Silva Santos Moreira, Review on geopolymers as wellbore sealants: state of the art optimization for CO_2 exposure and perspectives, ACS Omega 8 (26) (2023) 23320–23345, https://doi.org/10.1021/acsomega.3c01777.
[21] G. Franchin, P. Scanferla, L. Zeffiro, H. Elsayed, A. Baliello, G. Giacomello, M. Pasetto, P. Colombo, Direct ink writing of geopolymeric inks, J. Eur. Ceram. Soc. 37 (6) (2017) 2481–2489, https://doi.org/10.1016/j.jeurceramsoc.2017.01.030.
[22] A. Rincón, G. Giacomello, M. Pasetto, E. Bernardo, Novel ‘inorganic gel casting’ process for the manufacturing of glass foams, J. Eur. Ceram. Soc. 37 (5) (2017) 2227–2234, https://doi.org/10.1016/j.jeurceramsoc.2017.01.012.

[23] T. Iwaida, S. Nagasaki, S. Tanaka, T. Yaita, S. Tachimori, Structure alteration of C-S-H (calcium silicate hydrated phases) caused by sorption of caesium, Radiochim. Acta 90 (9–11) (2002) 677–681, https://doi.org/10.1524/ract.2002.90.9-11_2002.677.

[24] G. Bougueon, T. Kauss, B. Dessane, P. Barthelemy, S. Crauste-Manciet, Micro- and nano-formulations for bioprinting and additive manufacturing, Drug Discov. Today 24 (1) (2019) 163–178, https://doi.org/10.1016/j.drudis.2018.10.013.

[25] A. Dasan, J. Kraxner, L. Grigolato, G. Savio, H. Elsayed, D. Galusek, E. Bernardo, 3D printing of hierarchically porous lattice structures based on akermanite glass microspheres and reactive silicone binder, J. Funct. Biomater. 13 (1) (2022), https://doi.org/10.3390/jfb13010008.

[26] F.C. Figueira, A.M. Bernardin, Sinter-crystallization of spodumene LAS glass-ceramic tiles processed by single-firing, J. Alloy. Compd. 800 (2019) 525–531, https://doi.org/10.1016/j.jallcom.2019.06.107.

[27] H. Elasyed, A. Rincon Romero, G. Molino, C. Vitale Brovarone, E. Bernardo, Bioactive glass-ceramic foam scaffolds from 'inorganic gel casting' and sinter-crystallization, Materials 11 (3) (2018), https://doi.org/10.3390/ma11030349.

[28] J. Joo, Y. Ye, D. Kim, J. Lee, S. Jeon, Magnetically recoverable hybrid TiO_2 nanocrystal clusters with enhanced photocatalytic activity, Mater. Lett. 93 (2013) 141–144, https://doi.org/10.1016/j.matlet.2012.10.067.

[29] K.-Y.A. Lin, Z.-Y. Zhang, Degradation of bisphenol A using peroxymonosulfate activated by one-step prepared sulfur-doped carbon nitride as a metal-free heterogeneous catalyst, J. Chem. Eng. 313 (2017) 1320–1327, https://doi.org/10.1016/j.cej.2016.11.025.

[30] H. Elsayed, P. Colombo, E. Bernardo, Direct ink writing of wollastonite-diopside glass-ceramic scaffolds from a silicone resin and engineered fillers, J. Eur. Ceram. Soc. 37 (13) (2017) 4187–4195, https://doi.org/10.1016/j.jeurceramsoc.2017.05.021.

[31] R. Li, Y. Jia, N. Bu, J. Wu, Q. Zhen, Photocatalytic degradation of methyl blue using Fe_2O_3 /TiO_2 composite ceramics, J. Alloy. Compd. 643 (2015) 88–93, https://doi.org/10.1016/j.jallcom.2015.03.266.

[32] M.A.E. Wafi, M.A. Ahmed, H.S. Abdel-Samad, H.A.A. Medien, Exceptional removal of methylene blue and p-aminophenol dye over novel TiO_2/RGO nanocomposites by tandem adsorption-photocatalytic processes, Mater. Sci. Energy Technol. 5 (2022) 217–231, https://doi.org/10.1016/j.mset.2022.02.003.

[33] S.S. Al-Shamali, Photocatalytic degradation of methylene blue in the presence of TiO2 catalyst assisted solar radiation, Chem. Environ. Sci. (2013) https://api.semanticscholar.org/CorpusID:6465060.

[34] S. Moosavi, R.Y.M. Li, C.W. Lai, Y. Yusof, S. Gan, O. Akbarzadeh, Z.Z. Chowhury, X. G. Yue, M.R. Johan, Methylene blue dye photocatalytic degradation over synthesised Fe_3O_4/AC/TiO_2 nano-catalyst: degradation and reusability studies, Nanomater. (Basel) 10 (12) (2020), https://doi.org/10.3390/nano10122360.

[35] A.T. Adeleye, K.I. John, J.O. Ighalo, S. Ogunniyi, C.A. Adeyanju, A.G. Adeniyi, M. Elawad, M.O. Omorogie, Photocatalytic remediation of methylene blue using hydrothermally synthesized H-Titania and Na-Titania nanotubes, Heliyon 8 (12) (2022), e12610, https://doi.org/10.1016/j.heliyon.2022.e12610.

[36] H. Maleki, V. Bertola, TiO_2 nanofilms on polymeric substrates for the photocatalytic degradation of methylene blue, ACS Appl. Nano Mater. 2 (11) (2019) 7237–7244, https://doi.org/10.1021/acsanm.9b01723.